SCIENCE CHINA
Technological Sciences

• Article •

December 2014 Vol.57 No.12: 2407–2417
doi: 10.1007/s11431-014-5717-8

Dynamics of tether-tugging reorbiting with net capture

LIU HaiTao*, ZHANG QingBin, YANG LePing, ZHU YanWei & ZHANG YuanWen

College of Aerospace Science and Engineering, National University of Defense Technology, Changsha 410073, China

Received May 28, 2014; accepted October 3, 2014; published online November 6, 2014

To control the growth of space debris in the geostationary earth orbit (GEO), a novel solution of net capture and tether-tugging reorbiting is proposed. After capture, the tug (i.e., active spacecraft), tether, net, and target (i.e., GEO debris) constitute a rigid-flexible coupled tethered combination system (TCS), and subsequently the system is transported to the graveyard orbit by a thruster equipped on the tug. This paper attempts to study the dynamics of tether-tugging reorbiting after net capture. The net is equivalent to four flexible bridles, and the tug and target are viewed as rigid bodies. A sophisticated mathematical model is developed, taking into account the system orbital motion, relative motion of two spacecraft and spacecraft attitude motion. Given the complexity of the model, the numerical method is adopted to study the system dynamics characteristics. Particular attention is given to the investigation of the possible risks such as tether slack, spacecraft collision, tether rupture, tether-tug intertwist and destabilizing of the tug's attitude. The influence of the initial conditions and the magnitudes of the thrust are studied.

active debris removal, net capture, tether-tugging reorbiting, thruster, risk analysis

Citation: Liu H T, Zhang Q B, Yang L P, et al. Dynamics of tether-tugging reorbiting with net capture. Sci China Tech Sci, 2014, 57: 2407–2417, doi: 10.1007/s11431-014-5717-8

1 Introduction

The geostationary earth orbit (GEO) or, generally, the geosynchronous belt is a valuable but narrow zone with a growing number of large, defunct Earth sensing and communication satellites, as well as spent rocket bodies [1,2]. The debris at GEO, if not properly disposed, may occupy the GEO ring permanently owing to the high altitude and negligible atmospheric drag [3]. This accumulated effect makes the GEO resource quite scarce. To control the growth of space debris, numerous active debris removal (ADR) concepts have been conceived, covering a range of technologies such as robotic manipulators [4,5], laser systems [6], electrodynamic tethers [7,8] and space elevators [9], yet most of these have not been well thought out and many are not practical for implementation at GEO [10]. In recent years, several on-orbit capture and tether-tugging reorbiting systems, utilizing harpoons [11], mechanical grapples [12–14], or nets [15–17] attached at the end of the tether to grab the debris, have been suggested for ADR [10]. In general, these solutions seem much simpler to apply than previously mentioned ones, and the hazards associated with rendezvous and docking with non-cooperative tumbling objects are better avoided [18]. Among these on-orbit capture approaches, net capture, which has been demonstrated in the robotic geostationary orbit restorer (ROGER) [19], is especially promising for merits of high flexibility, large error tolerance, light weight, small package and long capture distance. After capture, the tug (i.e., active spacecraft), tether, net, and target (i.e., GEO debris) constitute a tethered combination system (TCS), which is rigid-flexible coupled (Figure 1). Subsequently the tug transports the target to the graveyard orbit by a thruster equipped on the tug, and then

*Corresponding author (email: lhtnudt@163.com)

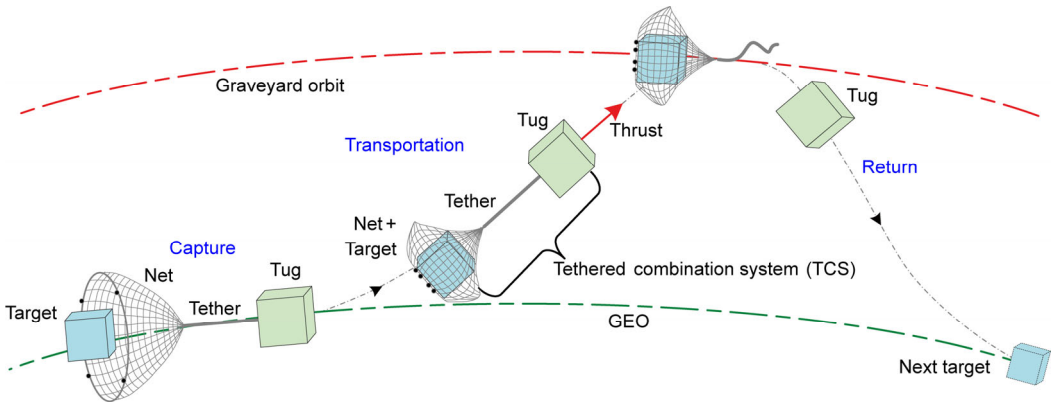

Figure 1 (Color online) Process of net capture and tether-tugging reorbiting.

returns to GEO for reuse.

Compared with traditional tethered satellite systems (TSS), TCS is provided with more complicated mechanical behaviors for the complex cable structure consisting of the tether and net, thus modeling and resolving such a nonlinear system is more challenging. Moreover, TSS generally moves on the Keplerian orbit [20–22], while TCS runs on the non-Keplerian orbit in the transportation phase. Therefore, the orbital movement must be taken into consideration when modeling TCS. In addition, TCS bears the features of short tether length, a centralized thrust acting on the tug and a weak GEO gravity gradient effect, consequently we should keep a watchful eye on such risks as tether slack, spacecraft collision, tether rupture, tether-tug intertwist and destabilizing of the tug's attitude.

Some researches on the dynamics of the tether-tugging issues have been carried out. Cho and McClamroch [23] proposed an optimal orbit transfer method for the tethered satellite by a continuous thrust applied on the active spacecraft. Sun, Zhao et al. [24,25] analyzed the librational and vibrational characteristics of the tethered system under a small, continuous and constant thrust, and investigated the stability and control of the tethered satellite in the orbital plane [26]. Liu et al. [27] proposed a four-phase tether-tugging reorbit scheme for defunct geostationary satellites. Jasper et al. [28] suggested utilizing fuel reserves on a recently launched upper stage to rendezvous with, tether, and deorbit the LEO debris, and applying thrust input shaping approach to reduce the post-burn relative motion of the tethered tug-debris system, thus reducing collision likelihood [29]. Aslanov et al. [30–32] studied the dynamics of deorbiting large space debris by means of a tethered space tug under the action of the space tug thruster. However, most of these researchers modeled spacecraft as mass points, ignoring the spacecraft attitude motion.

The aim of this paper is to study the dynamics of tether-tugging reorbiting after net capture. For simplicity, the net is equivalent to four flexible bridles which connect the four corners of the target and the end of the tether, and the tug and target are viewed as rigid bodies. Based on these assumptions, a sophisticated mathematical model is established, consisting of the system orbital motion, relative motion of two spacecraft and spacecraft attitude motion. Given the complexity of the model, the numerical method is taken to study the system dynamics characteristics. Particular attention is given to the investigation of the possible risks. The influence of the initial conditions and the magnitudes of the thrust are also studied.

2 Dynamic modeling

2.1 Basic assumption and reference frames

Given the extreme complexity of the net structure and the huge amount of the net nodes, it will bring heavy burden to solve the tether-tugging reorbiting dynamic model if we build the fine model for the net. To better analyze the reorbiting process of TCS and meanwhile reflect the basic features of the net structure, we establish a four-bridle and double-rigid-body model as shown in Figure 2, by referring to the research on the parachute recovery system [33,34]. The basic assumption is as follows: The tug and target are considered as rigid bodies; the net is treated as four flexible bridles, the longitudinal elasticity and damping of the tether and bridles are taken into account.

Denote spacecraft i ($i=1,2$) as the tug and target respectively and bridle j ($j=1,2,3,4$) as the four bridles respectively. Let P_1 be the tether attaching point to the tug, P_2 the tether-bridle confluence point, D_j the suspension point of bridle j on the target, $\boldsymbol{l}=\overrightarrow{P_1P_2}$ the tether vector, $\boldsymbol{D}_j=\overrightarrow{D_jP_2}$ the bridle vector, $\boldsymbol{\rho}_1$ the position vector from P_1 to the centroid of tug O_1, $\boldsymbol{\rho}_2$ the position vector from P_2 to the centroid of tug O_2, $\boldsymbol{F}_c$ the thrust of the tug, and $\boldsymbol{M}_c$ the control moment of the tug. Three reference frames are introduced as follows:

(1) The Earth-centered inertial reference frame $\mathcal{N}$, with

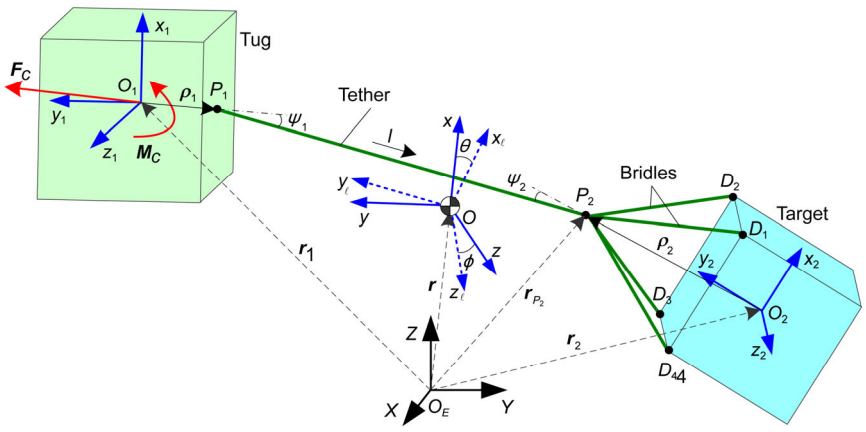

Figure 2 (Color online) The four-bridle and double-rigid-body model.

its origin attached to the Earth center O_E, X-axis pointing to vernal equinox, Z-axis perpendicular to the equatorial plane and pointing to the north pole, and Y-axis determined by the right-hand rule.

(2) The orbital reference frame $\mathcal{H}$, with its origin attached to the system centroid O, x-axis pointing from O_E to O, z-axis along the positive normal of the osculating orbit, and y-axis perpendicular to x-axis in the osculating plane and pointing to the motion direction.

(3) The body fixed frame $\mathcal{B}_i$, with its origin attached to O_i which is the centroid of spacecraft i, and three coordinate axes x_i, y_i and z_i fixed to the principal axes of inertia and satisfying the right-hand rule.

Define the 3-1-2 Euler angle from $\mathcal{B}_i$ to $\mathcal{H}$ as the pitch angle α_i, the yaw angle β_i and the roll angle γ_i, and define $\boldsymbol{\Psi}_i=[\alpha_i,\beta_i,\gamma_i]^{\mathrm{T}}$. After transforming $\mathcal{H}$ by performing a 3-1 Euler rotation sequence through the angles θ and φ (Figure 2), if the new $-y_\ell$-axis points along tether vector $\boldsymbol{l}$, then the angles θ and φ are named in- and out-of-plane swing angles of the tether relative to $\mathcal{H}$. According to the definition, we obtain

$$\boldsymbol{l}=[ls_\theta c_\varphi,-lc_\theta c_\varphi,-ls_\varphi]^{\mathrm{T}}, \tag{1}$$

where $c_{(\cdot)}$ denotes $\cos(\bullet)$ and $s_{(\cdot)}$ denotes $\sin(\bullet)$, similarly hereinafter.

Let ψ_1 be the angle between the tether and tug, and ψ_2 the angle between the tether and target (Figure 2). Define

$$\psi_1=\arccos\left(\frac{\boldsymbol{l}\bullet\boldsymbol{\rho}_1}{l\rho_1}\right),\quad \psi_2=\arccos\left(-\frac{\boldsymbol{l}\bullet\boldsymbol{\rho}_2}{l\rho_2}\right). \tag{2}$$

2.2 Dynamics equation

Let $\boldsymbol{r}_i$, $\boldsymbol{r}$ be the position vector of spacecraft i and system centroid in $\mathcal{N}$, then according to the Newton second law, there exist in $\mathcal{N}$:

$$\ddot{\boldsymbol{r}}_1=-\frac{\mu}{r_1^3}\boldsymbol{r}_1+\frac{\boldsymbol{F}_c+\boldsymbol{T}}{m_1}+\boldsymbol{f}_{d1}, \tag{3}$$

$$\ddot{\boldsymbol{r}}_2=-\frac{\mu}{r_2^3}\boldsymbol{r}_2+\frac{1}{m_2}\sum_{j=1}^{4}\boldsymbol{T}_j+\boldsymbol{f}_{d2}, \tag{4}$$

$$\ddot{\boldsymbol{r}}=\frac{1}{m}\left(-\frac{\mu m_1\boldsymbol{r}_1}{r_1^3}-\frac{\mu m_2\boldsymbol{r}_2}{r_2^3}+\boldsymbol{F}_c\right)+\boldsymbol{f}_d, \tag{5}$$

where μ represents earth's gravitational constant, m_i the mass of spacecraft i, $m=m_1+m_2$ the mass of system, $\boldsymbol{T}$ the tether tension, $\boldsymbol{T}_j$ the tension of bridle j, and $\boldsymbol{f}_{di}$, $\boldsymbol{f}_d$ the disturbing acceleration acting on spacecraft i and system centroid respectively [35].

Let $\boldsymbol{d}=\boldsymbol{r}_2-\boldsymbol{r}_1$ be the position vector from the tug to target, then combining eqs. (3) and (4) yields the expression in $\mathcal{N}$:

$$\ddot{\boldsymbol{d}}=\ddot{\boldsymbol{r}}_2-\ddot{\boldsymbol{r}}_1=\frac{\mu}{r_1^3}\boldsymbol{r}_1-\frac{\mu}{r_2^3}\boldsymbol{r}_2-\frac{\boldsymbol{F}_c}{m_1}-\frac{\boldsymbol{T}}{m_1}+\frac{1}{m_2}\sum_{j=1}^{4}\boldsymbol{T}_j+\Delta\boldsymbol{f}_d, \tag{6}$$

where $\Delta\boldsymbol{f}_d$ is the relative disturbing acceleration. Transforming eq. (6) into $\mathcal{H}$, we can obtain the relative motion dynamics equation in $\mathcal{H}$ [36]:

$$\begin{aligned}\ddot{\boldsymbol{d}}=&-\dot{\boldsymbol{\omega}}\times\boldsymbol{d}-2\boldsymbol{\omega}\times\dot{\boldsymbol{d}}-\boldsymbol{\omega}\times(\boldsymbol{\omega}\times\boldsymbol{d})\\&+\frac{\mu}{r_1^3}\boldsymbol{r}_1-\frac{\mu}{r_2^3}\boldsymbol{r}_2-\frac{\boldsymbol{F}_c}{m_1}-\frac{\boldsymbol{T}}{m_1}+\frac{1}{m_2}\sum_{j=1}^{4}\boldsymbol{T}_j+\Delta\boldsymbol{f}_d,\end{aligned} \tag{7}$$

where $\boldsymbol{\omega}$ is the angular velocity of the osculating orbit of the system.

It is worth noting that $(\boldsymbol{r}_1,\boldsymbol{r}_2)$ and $(\boldsymbol{r},\boldsymbol{d})$ can be expressed by each other, satisfying

$$\boldsymbol{r}=\eta_1\boldsymbol{r}_1+\eta_2\boldsymbol{r}_2,\ \ \boldsymbol{d}=\boldsymbol{r}_2-\boldsymbol{r}_1, \tag{8}$$

$$\boldsymbol{r}_1=\boldsymbol{r}-\eta_2\boldsymbol{d},\ \ \boldsymbol{r}_2=\boldsymbol{r}+\eta_1\boldsymbol{d}, \tag{9}$$

where $\eta_i=m_i/m$ is the mass ratio of spacecraft i. For TCS in GEO, it may cause great calculation error if the relative position is computed by $\boldsymbol{d}=\boldsymbol{r}_2-\boldsymbol{r}_1$ since there exists $r_1\approx r_2\gg d$. Therefore $(\boldsymbol{r},\boldsymbol{d})$ is chosen as the state variable in the dynamics equation, and $(\boldsymbol{r}_1,\boldsymbol{r}_2)$ is calculated by eq. (9).

Let $\boldsymbol{\omega}_i=[\omega_{ix},\omega_{iy},\omega_{iz}]^{\mathrm{T}}$ be the absolute angular velocity of spacecraft i in $\mathcal{B}_i$. According to the Euler kinematical equation, we obtain

$$\boldsymbol{\omega}_i=\begin{bmatrix}-\dot{\alpha}_i c_{\beta_i}s_{\gamma_i}+\dot{\beta}_i c_{\gamma_i}-\omega c_{\beta_i}s_{\gamma_i}\\ \dot{\alpha}_i s_{\beta_i}+\dot{\gamma}_i+\omega s_{\beta_i}\\ \dot{\alpha}_i c_{\beta_i}c_{\gamma_i}+\dot{\beta}_i s_{\gamma_i}+\omega c_{\beta_i}c_{\gamma_i}\end{bmatrix}. \tag{10}$$

According to the Euler dynamics equation, we obtain

$$\begin{cases}\boldsymbol{I}_1\dot{\boldsymbol{\omega}}_1+\boldsymbol{\omega}_1\times\boldsymbol{I}_1\boldsymbol{\omega}_1=\boldsymbol{M}_c+\boldsymbol{M}_{T1}+\boldsymbol{M}_{d1},\\ \boldsymbol{I}_2\dot{\boldsymbol{\omega}}_2+\boldsymbol{\omega}_2\times\boldsymbol{I}_2\boldsymbol{\omega}_2=\boldsymbol{M}_{T2}+\boldsymbol{M}_{d2},\end{cases} \tag{11}$$

where $\boldsymbol{I}_i=diag(I_{ix},I_{iy},I_{iz})$ is inertia matrix of spacecraft i represented in $\mathcal{B}_i$, $\boldsymbol{M}_c=[M_{cx},M_{cy},M_{cz}]^{\mathrm{T}}$ the tug's control moment represented in $\mathcal{B}_1$, $\boldsymbol{M}_{di}$ the disturbing torque acting on spacecraft i represented in $\mathcal{B}_i$, and $\boldsymbol{M}_{Ti}$ the moment of tension acting on spacecraft i represented in $\mathcal{B}_i$, satisfying

$$\boldsymbol{M}_{T1}=\boldsymbol{\rho}_1\times\boldsymbol{T},\ \boldsymbol{M}_{T2}=\sum_{j=1}^{4}\boldsymbol{D}_j\times\boldsymbol{T}_j. \tag{12}$$

In addition, the tug's mass may decrease due to fuel consumption during reorbiting, satisfying

$$\dot{m}_1=-\frac{|\boldsymbol{F}_c|}{I_{sp}g_e}, \tag{13}$$

where I_{sp} represents the specific impulse and g_e is the gravitational acceleration at the surface of the Earth.

Hence the dynamics equation of tether-tugging reorbiting is deduced, including the system orbital motion eq. (5), relative motion eq. (7), spacecraft attitude motion eq. (11) and differential of the tug's mass eq. (13).

2.3 Tension solution

The tether and bridles are flexible and easy to go slack, so the key to resolve the four-bridle and double-rigid-body model is to determine the tension of the tether and bridles. Taking the tether-bridle confluence point as a particle with a small mass, we obtain the dynamics equation of the particle as

$$m_{P_2}\ddot{\boldsymbol{r}}_{P_2}=-\boldsymbol{T}-\sum_{j=1}^{4}\boldsymbol{T}_j=-T\boldsymbol{n}_l-\sum_{j=1}^{4}T_j\boldsymbol{n}_{l_j}, \tag{14}$$

where m_{P_2} is the mass of the particle, $\boldsymbol{r}_{P_2}$ the position vector of the particle in $\mathcal{N}$, $\boldsymbol{n}_l$ and $\boldsymbol{n}_{l_j}$ the unit vector of the tether and bridle j respectively. The tension of the tether and bridles can be approximated as the sum of linear spring and damper, satisfying

$$T=\begin{cases}k(l-\tilde{l})+c\dot{l}, & l>\tilde{l},\\ 0, & l\leqslant\tilde{l},\end{cases} \tag{15}$$

$$T_j=\begin{cases}k_j(l_j-\tilde{l}_j)+c_j\dot{l}_j, & l_j>\tilde{l}_j,\\ 0, & l_j\leqslant\tilde{l}_j,\end{cases} \tag{16}$$

$$l=\left\|\boldsymbol{r}_{P_2}-\boldsymbol{r}_{P_1}\right\|,\ \ \boldsymbol{n}_l=\left(\boldsymbol{r}_{P_2}-\boldsymbol{r}_{P_1}\right)/l,\ \ \dot{l}=\left(\dot{\boldsymbol{r}}_{P_2}-\dot{\boldsymbol{r}}_{P_1}\right)\bullet\boldsymbol{n}_l, \tag{17}$$

$$l_j=\left\|\boldsymbol{r}_{P_2}-\boldsymbol{r}_{D_j}\right\|,\ \ \boldsymbol{n}_{l_j}=\left(\boldsymbol{r}_{P_2}-\boldsymbol{r}_{D_j}\right)/l_j,\ \ \dot{l}_j=\left(\dot{\boldsymbol{r}}_{P_2}-\dot{\boldsymbol{r}}_{D_j}\right)\bullet\boldsymbol{n}_{l_j}, \tag{18}$$

where l and $\dot{l}$ represent the actual length of the tether and its differential, $\tilde{l}$ the original length of the tether, k and c the spring coefficient and damping coefficient of the tether, l_j and $\dot{l}_j$ the actual length of bridle j and its differential, $\tilde{l}_j$ the original length of bridle j, k_j and c_j spring coefficient and damping coefficient of bridle j, $\boldsymbol{r}_{P_1}$ the position vector of P_1 in $\mathcal{N}$, and $\boldsymbol{r}_{D_j}$ the position vector of D_j in $\mathcal{N}$.

Adding eqs. (14)–(18) to the dynamics equation of the system, we obtain the position and velocity of P_2, and work out the tension of the tether and bridles by eqs. (15) and (16).

3 Numerical simulation and analysis

3.1 Parameters of simulation

Considering the complexity of the dynamic model, the numerical method is adopted to study the system dynamics characteristics. In view of the practical requirement of the reorbiting mission, the thrust is set to be constant along the circumference of the orbit [37]. Note that such active control methods as the attitude control of the tug, relative motion control of two spacecraft and tether tension control are out of discussion in this paper, and we focus on system dynamics under the actuation of thruster. Simulation parameters are presented in Table 1. Referring to the GEO debris

Table 1 Parameters of simulation

Parameter	Value
Orbital radius of GEO a_0	42164 m
Perigee radius increment of the graveyard orbit ΔH	300 km
Earth's gravitational constant μ	3.986×10^{14} m^3/s^2
Constant circumferential thrust F	0.5 N/2 N/10 N
Specific impulse I_{sp}	296 s
Initial mass of the tug m_{10}	1000 kg
Mass of the target m_2	2500 kg
Inertia matrix of the tug $\boldsymbol{I}_1$	diag(400,420,350) kg m^2
Inertia matrix of the target $\boldsymbol{I}_2$	diag(2500,3000,2000) kg m^2
Position vector of P_1 relative to the tug $\boldsymbol{\rho}_1$	$[0,-1,0]^{\mathrm{T}}$ m
Original length of the tether $\tilde{l}$	100 m
Young's modulus of the tether E	75 GPa
Diameter of the tether D	1 mm
Tensile strength of the tether σ_u	3.32 GPa
Spring coefficient k, k_j	589 N/m
Damping coefficient c, c_j	104 N s m^{-1}
Four suspension points of the bridles in $\mathcal{B}_2$	[2,2,10], [2,2,–10], [–2,2,–10], [–2,2,10]
Original length of the bridles $\tilde{l}_1-\tilde{l}_4$	14 m, 14 m, 14 m, 14 m

Table 2 Reference states

Parameter	Value
Orbital elements of system $(a,e,i,\varpi,\Omega,\nu)$	(42164 km,0,0,0,0,0)
Euler angles of the tug $\boldsymbol{\Psi}_1$	$[0,0,0]^{\mathrm{T}}$
Euler angles of the target $\boldsymbol{\Psi}_2$	$[0,0,0]^{\mathrm{T}}$
Angular velocity of the tug $\boldsymbol{\omega}_1$	$[0,0,0]^{\mathrm{T}}$ °/s
Angular velocity of the target $\boldsymbol{\omega}_2$	$[0,0,0]^{\mathrm{T}}$ °/s
Tether elongation and swing angles $[\Delta l,\theta,\varphi]^{\mathrm{T}}$	$[0,\mathrm{m},0,0]^{\mathrm{T}}$
Original length of the bridles $\tilde{l}_1-\tilde{l}_4$	14 m, 14 m, 14 m, 14 m

disposal advice of the Inter-Agency Space Debris Coordination Committee (IADC) [38], we define the graveyard orbit as one whose perigee radius is 300 km above GEO. Three magnitudes of thrust, 0.5, 2 and 10 N, are taken into account. The initial tug mass is 1000 kg, the target mass is 2500 kg, and the original length is 100 m. Since the target is equipped with solar panels, we approximate the target as a $20\ \mathrm{m}\times4\ \mathrm{m}\times4\ \mathrm{m}$ cuboid and assume its four vertexes as the suspension points.

During the tether-tugging process, the following issues are emphasized in the simulation: whether the tug's attitude is stable, whether the target collides with the tug, whether the tether intertwines with the tug, whether the tether ruptures, and whether the tether and bridles go slack. The J_2 perturbation has been taken into account in the simulation.

3.2 Reorbiting process in the reference states

The gravity-gradient effect makes the tethered satellite systems stable along local vertical [39], and the gravity-gradient force can be approximated to $F_{GG}=3m\omega^2L$. For TCS in this paper, the gravity-gradient force is about 0.001 N, which is far smaller than the thrust. Therefore for TCS under the actuation of a constant circumferential thrust, the orientation of the equilibrium does not point along local vertical anymore; instead, it is along the circumference of the orbit [24]. Hence we define the reference states as shown in Table 2, in which the system lies in GEO, the Euler angles of two spacecraft are all zeros, the tether is along the circumference of the orbit, the tether and bridles are straight without any initial tension, and there is no initial relative velocity between the tug and target.

Supposing the initial state is identical with the reference states and the thrust has a value of 0.5 N, the reorbiting process is shown in (Figure 3. As shown in (Figure 3(a), the tension of the tether and bridles fluctuates when the thrust is first applied, and eventually goes steady due to the damping effect. It is worth noting that the eventual value of tether tension, 0.357 N, is consistent with $T=F\eta_2$. We also figure out that the tension of the tether and bridles is positive all the time and the maximum is less than 0.7 N, which means there are no risks of tether slack and tether rupture. In Figure 3(b), the tether elongation eventually stabilizes to 6.06×10^{-4} m after a short fluctuation, which is consistent with $EA\Delta l=F\eta_2$. We also note that the tether is always tight, the in-plane angle varies with an amplitude of $0.01°$ and the out-of-plane angle is nearly zero, which indicates that there are no risks of spacecraft collision and TCS can keep stable along circumference of the orbit. In Figure 3(c) and (d), the amplitude of the Euler angles of two spacecraft is smaller than $0.2°$ and that of the angles between the tether and spacecraft is also smaller than $0.2°$, which means that the attitude of the tug and target can keep stable.

Without changing other simulation parameters, we assume the terminal condition as the perigee of the system being promoted 300 km above GEO, then we obtain the entire reorbiting process from GEO to graveyard orbit as shown in Figure 4. In Figure 4(a), the apogee radius r_a, the semi-major axis a and the perigee radius r_p all increase gradually, and finally the perigee radius increases by 300 km at the terminal time 22.59 h, which means that the constant circumferential thrust can satisfy the reorbiting requirement of TCS. Figure 4(b) is the time history of the in-plane swing angle, the pitch angle of the tug and target respectively. It is apparent that the long-term motion of the three angles shares the same period with the orbit motion, which is due to the coupling effect of the orbit motion with the tether pendular motion and the spacecraft attitude motion. However, the coupling effect is extremely small, with the tether swing angle fluctuating smaller than $0.1°$ and the pitch angles of the spacecraft smaller than $0.2°$, which

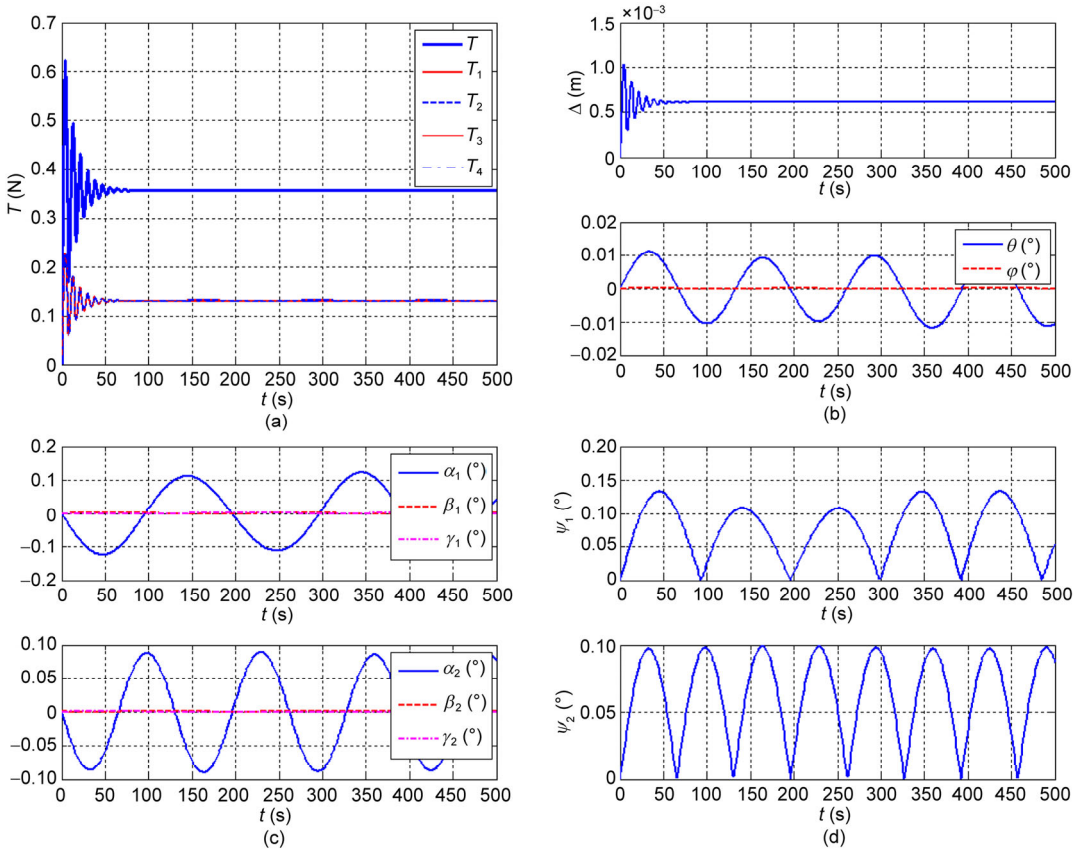

Figure 3 (Color online) Reorbiting process in the reference states (F = 0.5 N). (a) Tension of the tether and bridles; (b) tether elongation and swing angles; (c) Euler angles of two spacecraft; (d) angles between the tether and spacecraft.

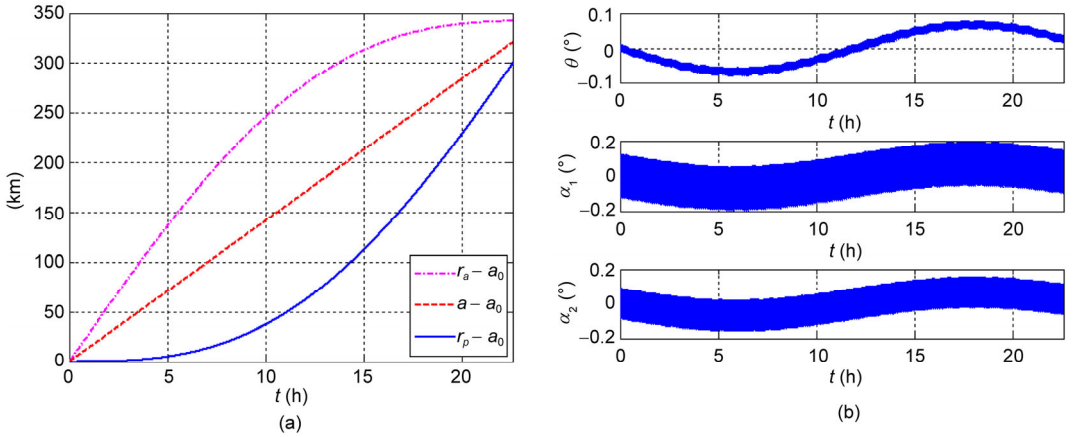

Figure 4 (Color online) The entire reorbiting process from GEO to graveyard orbit (F = 0.5 N). (a) Increment of system orbit parameter; (b) in-plane swing angle and pitch angles.

means in the reference states, the constant circumferential thrust can keep the system stable all along the entire reorbiting process.

Table 3 shows the reorbiting duration t_f and the fuel consumption m_p under different thrusts, where the fuel consumption is calculated by $m_p = m_{10} - m_1(t_f)$. We can make out that the greater the thrust is, the shorter the reorbiting duration is, and the more the fuel consumption is.

3.3 Influence of initial deviation on the reorbiting process

In the actual reorbiting process, the initial state may deviate from the reference states. For example, the target has an initial angular velocity (Case 1); the two spacecraft have an

Table 3 The reorbiting time and fuel consumption under different thrusts

F(N)	t_f(h)	m_p (kg)
0.5	22.59	14.04
2	12.88	32.00
10	7.26	90.13

initial transversal relative velocity (Case 2); or the two spacecraft have an initial longitudinal relative velocity (Case 3). These initial deviations may disturb system stability, even resulting in mission failure. The influence of initial deviations is examined respectively as follows.

Case 1.

Assuming the target has an initial angular velocity $\boldsymbol{\omega}_{20} = \pi/180 \times [0,0,0.5]^{\mathrm{T}}$; the thrust is 0.5 N; and other initial conditions are the same with the reference states, the reorbiting process is shown in Figure 5. As shown in Figure 5(a) and (b), the Euler angles of two spacecraft fluctuate greatly, and the angles between the tether and spacecraft are also big, among which the amplitude of the pitch of the tug reaches up to 32°, indicating possible risks of destabilization of the tug's attitude. In Figure 5(c), the tether elongation is always positive, indicating no risk of spacecraft collision. The tether has an in-plane pendular motion within 1.4°, due to the coupling effect of the spacecraft attitude motion with the tether pendular motion. In Figure 5(d), the tether tension is always positive and the maximum is smaller than 2.2 N, which means there are no risks of tether slack and tether rupture. The tension of bridle 1 and bridle 2 is almost overlapping and that of bridle 3 and bridle 4 is almost overlapping too. It is worth noting that all the four bridles experience such a moment when the tension is 0, which means that the bridle goes slack due to the revolution of the target.

From the simulation results above, we conclude that the initial angular velocity of the target greatly disturbs the attitude of two spacecraft. Now we study the influence of different initial angular velocities and different thrusts on the angles between the tether and spacecraft. When the target has different initial angular velocities, Figure 6 indicates that the greater the initial angular velocity is, the greater the angles between the tether and spacecraft are, which translates to greater likelihood for the system to be unstable. Especially when the initial angular velocity rises to 2°/s, the angle of the tether and tug exceeds 90°, which means the tether may intertwine with the tug. Under the actuation of different thrusts, Figure 7 denotes that the greater the thrust is, the smaller the angles between the tether and spacecraft are, which means that a great thrust is beneficial to the stabilization of spacecraft attitude.

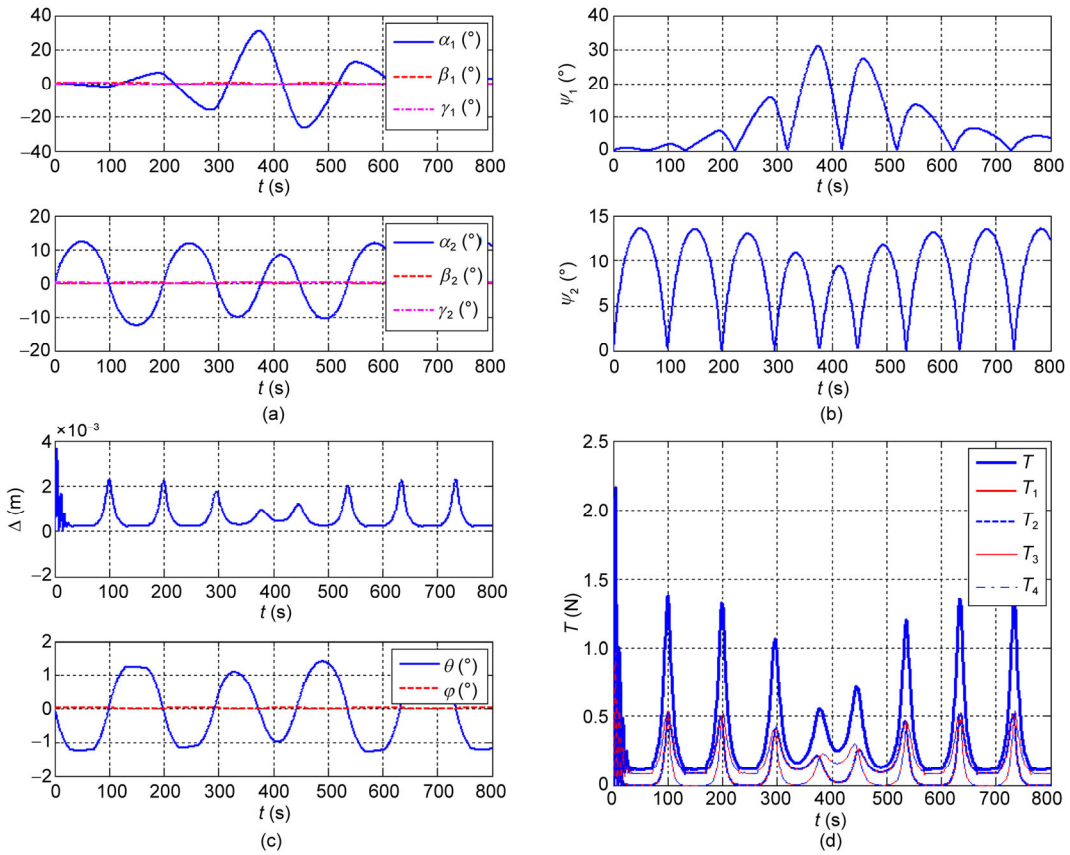

Figure 5 (Color online) The reorbiting process when the target has an initial angular velocity of 0.5°/s (F = 0.5 N). (a) Euler angles of two spacecraft; (b) angles between the tether and spacecraft; (c) tether elongation and swing angles; (d) tension of the tether and bridles.

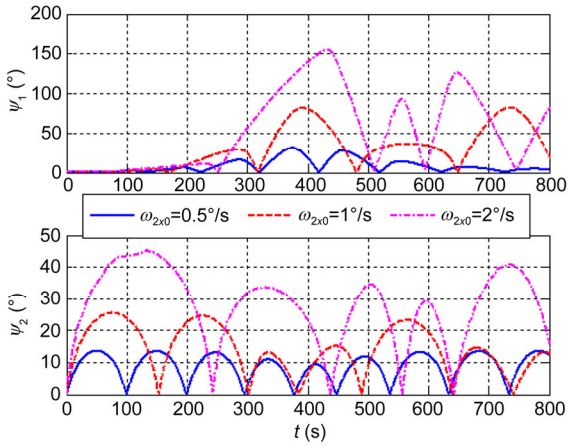

Figure 6 (Color online) Angles between the tether and spacecraft when the target has different initial angular velocities (F = 0.5 N).

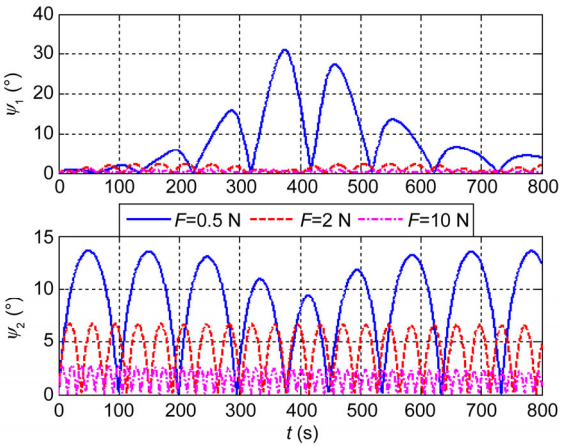

Figure 7 (Color online) Angles between the tether and spacecraft under the actuation of different thrusts (ω_{2x0} = 0.5°/s).

Case 2.

Supposing the two spacecraft have initial transversal (vertical to the tether) relative velocity $\dot{\boldsymbol{d}}_0 = [0.1, 0, 0]^{\mathrm{T}}$ m/s; the thrust is 0.5 N; and other initial conditions are the same with the reference states, the reorbiting process is shown in Figure 8. As shown in Figure 8(a) and (b), the tether swings in the orbit plane around 0°, with an amplitude of 24.5° and a period of 3020 s. It is apparent that the tether is always tight; the tension of the tether and bridles is always positive and the maximum is smaller than 0.8 N. These results indicate that there are no risks of spacecraft collision, tether rupture, tether slack and bridle slack. In Figure 8(c) and (d), we figure out that the change rule of the pitch angles of the tug and target is almost identical with the tether

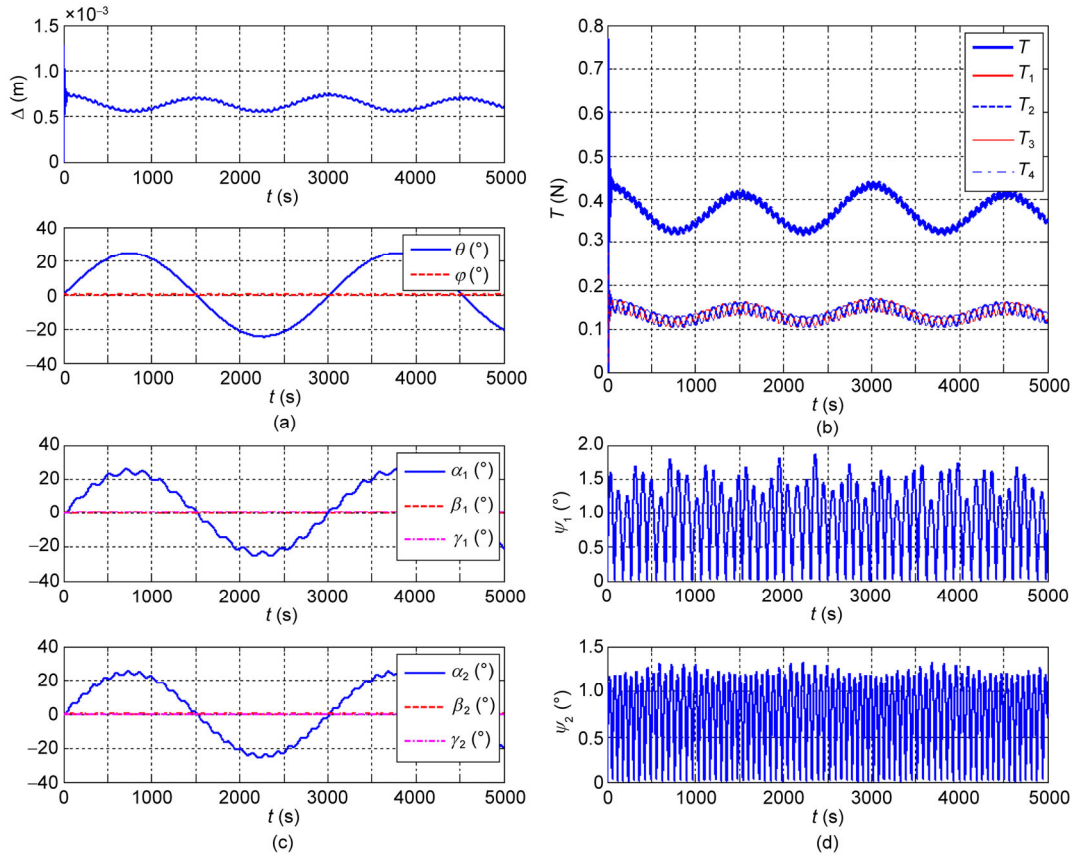

Figure 8 (Color online) The reorbiting process when the two spacecraft have initial transversal relative velocities of 0.1 m/s (F = 0.5 N). (a) Tether elongation and swing angles; (b) tension of the tether and bridles; (c) Euler angles of two spacecraft; (d) angles between the tether and spacecraft.

in-plane swing angle, but the angles between the tether and spacecraft are smaller than 2°. This is because the moment of tension makes the spacecraft attitude align with the tether, indicating the strong coupling effect of the tether with the spacecraft attitude.

From the simulation results above, we conclude that the initial transversal relative velocity of two spacecraft disturbs the tether swing angle greatly. Now we study the influence of different initial transversal relative velocities and different thrusts on the tether swing angle. When the two spacecraft have different initial transversal relative velocities, Figure 9 shows that the greater the initial transversal relative velocity is, the greater the tether swing angle is. Especially when the initial transversal relative velocity rises to 0.6 m/s, TCS becomes spinning. Under the actuation of different thrusts, Figure 10 denotes that the greater the thrust is, the smaller the tether swing angle is, and the greater the swing frequency is.

Case 3.

Assuming the two spacecraft have initial longitudinal (along to the tether) relative velocity $\dot{\boldsymbol{d}}_0 = [0, -0.1, 0]^{\mathrm{T}}$ m/s; the thrust is 2 N, and other initial conditions are the same with the reference states, the reorbiting process is shown in Figure 11. A course of impact and springback of the tether is shown in Figure 11(a). The impact process lasts for a period of 4.2 s, during which the peak of the tension is up to 47.5 N. Then the tether rebounds and two spacecraft get close to each other, and the tether tension is zero. If we ignore the gravitation during this short time, the relative motion can be viewed as uniformly retarded motion under the actuation of the thrust. The distance of two spacecraft will reach to a minimum $d_{\min}$, then gradually increase until the tether is tautened and next course of impact and springback comes up. In Figure 11(b), it is apparent that the tether tension and distance between two spacecraft both get stable after several courses of impact and springback. In Figure 11(c) and (d), the Euler angles of two spacecraft fluctuate greatly, and the angles between the tether and spacecraft are also big, among which the amplitude of the pitch of the tug reaches up to 23°, indicating possible risks of destabilization of the tug's attitude.

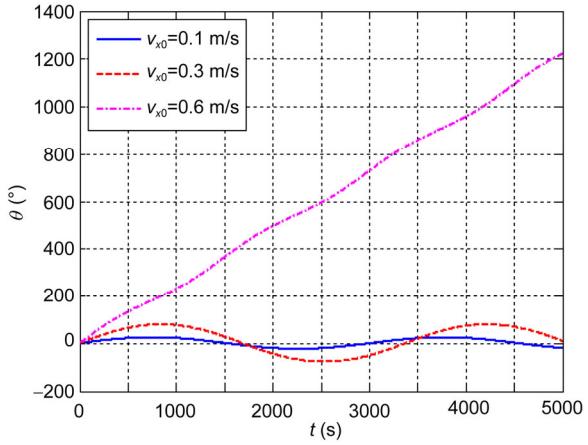

Figure 9 (Color online) The in-plane swing angle when the two spacecraft have different initial transversal relative velocities (F = 0.5 N).

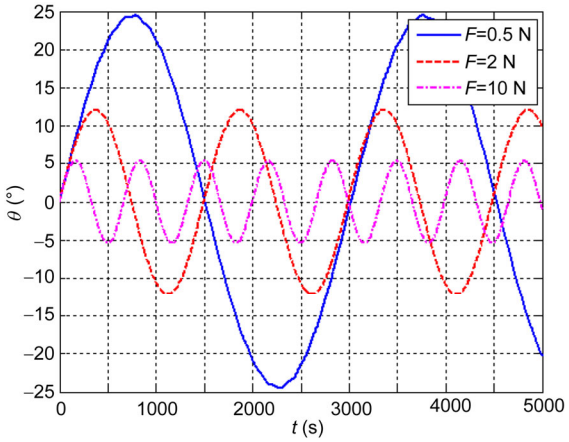

Figure 10 (Color online) The in-plane swing angle under the actuation of different thrusts (v_{x0} = 0.1 m/s).

From the simulation results above, we conclude that the initial longitudinal relative velocity of two spacecraft disturbs system stability greatly. It may cause tether rupture, tether slack, spacecraft collision after tether rebound, and spacecraft attitude instability. Figure 12 shows two examples of overlarge longitudinal relative velocity causing tether rupture and spacecraft collision, when the thrust remains 2 N. In case A, the longitudinal relative velocity is 5.5 m/s, and the peak of tether tension is up to the rupture load, defined as $F_{\mathrm{break}} = A\sigma_u = 2607.5$ N. In case B, the longitudinal relative velocity is 0.81 m/s, and the minimum distance $d_{\min}$ is smaller than the safe distance, defined as $D_{\mathrm{safe}} = 20$ m, resulting in spacecraft collision. Figure 13 shows the distance between two spacecraft under the actuation of different thrusts. It is obvious that the greater the thrust is, the smaller the tether rebound is, and the sooner the distance goes stable.

4 Conclusion

Based on the four-bridle and double-rigid-body assumption, a sophisticated mathematical model is developed to study the dynamics of tether-tugging reorbiting after net capture.

Compared with the usual dumbbell model, this model is more faithful for merits of better analysis of the system orbital motion, relative motion of two spacecraft and spacecraft attitude motion. The transportation process is simulated and analyzed on the premise that no active control but only a constant circumferential thrust is applied. The simulation results indicate that when the system is in the reference states, which means zero angular disturbances of two spacecraft, zero initial elongation of the tether and bridles,

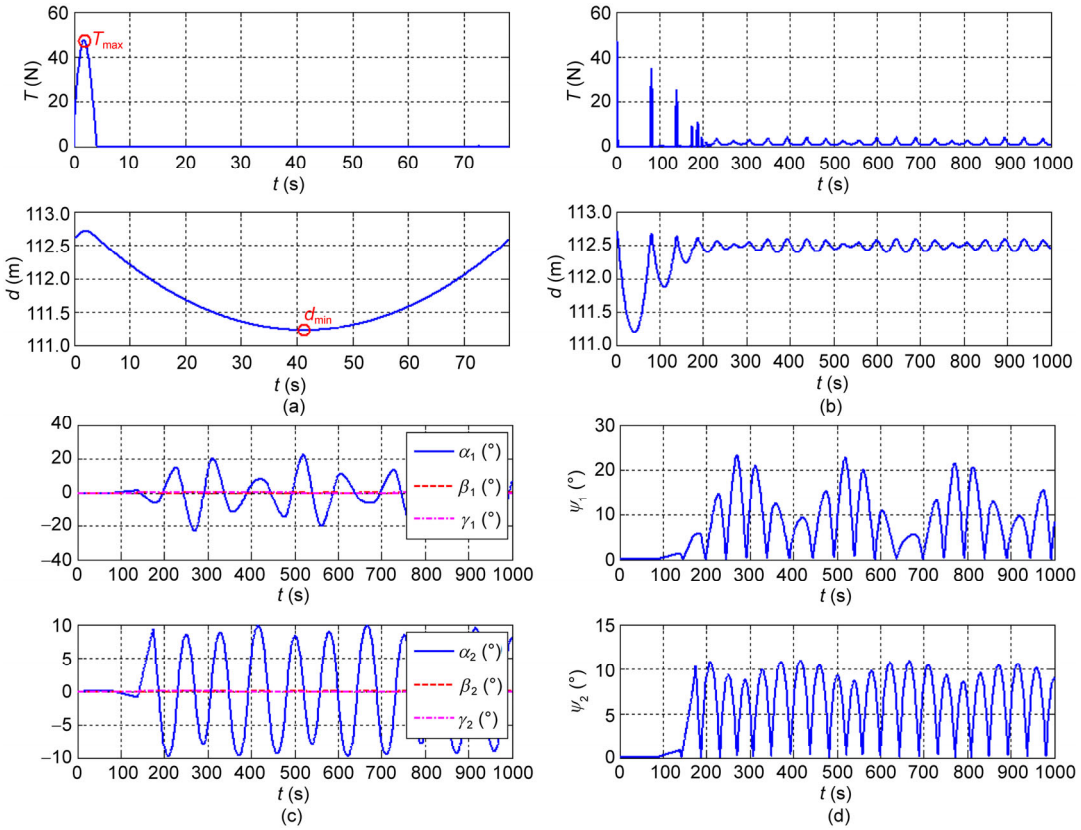

Figure 11 (Color online) The reorbiting process when the two spacecraft have initial longitudinal relative velocities of 0.1 m/s (F = 2 N). (a) A course of impact and springback of the tether; (b) tether tension and distance between two spacecraft; (c) Euler angles of two spacecraft; (d) angles between the tether and spacecraft.

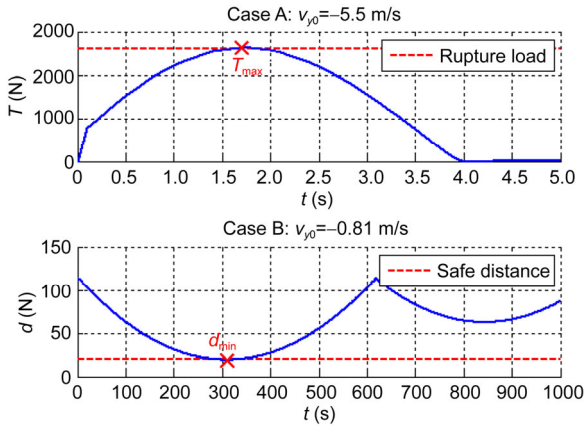

Figure 12 (Color online) Overlarge longitudinal relative velocity causes tether rupture and spacecraft collision (F = 2 N).

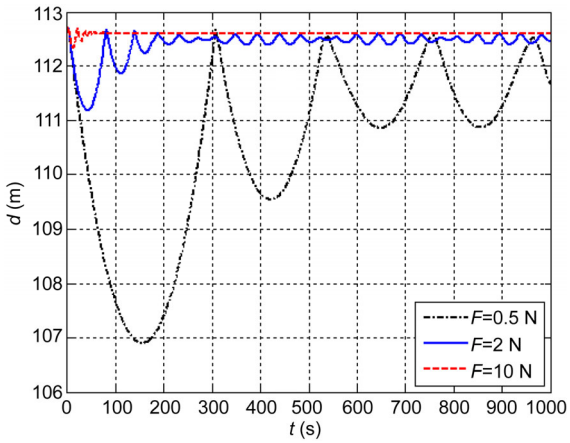

Figure 13 (Color online) Distance between two spacecraft under the actuation of different thrusts (v_{y0} = –0.1 m/s).

etc., the system can keep stable and the reorbiting mission of transferring the system into the graveyard orbit can be fulfilled successfully. The initial deviation of the reference states has remarkable influence on the system stability, and if the initial deviation is large, some risks may occur. A bigger thrust facilitates quicker reorbit and higher stability, yet consuming more fuel. The model and analysis results provide a substantial foundation for further reorbiting control of tethered combination system.

This work was supported by the National Natural Science Foundation of China (Grant No. 11272345).

1 Jehn R, Agapov V, Hernández C. The Situation in the geostationary Ring. Adv Space Res, 2005, 35: 1318–1327

2 Li H N, Gao Z Z, Li J S, et al. Mathematical prototypes for collocating geostationary satellites. Sci China Tech Sci, 2013, 56: 1086–1092
3 Smith D A, Martin C, Kassebom M, et al. A mission to preserve the geostationary region. Adv Space Res, 2004, 34: 1214–1218
4 Li Y H, Yang K Z, Shan C S, et al. A preliminary study on dead geostationary satellite removal. Sci China Tech Sci, 2010, 53: 3389–3396
5 Castronuovo M M. Active space debris removal—a preliminary mission analysis and design. Acta Astronaut, 2011, 69: 848–859
6 Phipps C R, Reilly J P. Orion: Clearing near-earth space debris in two years using a 30-Kw repetitively-pulsed laser. In: SPIE Proceedings of the International Society for Optical Engineering. SPIE, 1997
7 Ishige Y, Kawamoto S, Kibe S. Study on electrodynamic tether system for space debris removal. Acta Astronaut, 2004, 55: 917–929
8 Kawamoto S, Makida T, Sasaki F, et al. Precise numerical simulations of electrodynamic tethers for an active debris removal system. Acta Astronaut, 2006, 59: 139–148
9 Chobotov V, Melamed N, Ailor W H, et al. Ground assisted rendezvous with geosynchronous satellites for the disposal of space debris by means of Earth-oriented tethers. Acta Astronaut, 2009, 64: 946–951
10 Kaplan M H, Boone B, Brown R, et al. Engineering Issues for All Major Modes of in Situ Space Debris Capture. In: Proceedings of the AIAA SPACE 2010 Conference & Exposition. Anaheim: AIAA, 2010
11 Cougnet C, Alary D, Gerber B, et al. The Debritor: An “off the shelf” based multimission vehicle. In: Proceedings of 63rd International Astronautical Congress. Naples, Italy: IAC, 2012
12 Mankala K K, Agrawal S K. Dynamic modeling and simulation of impact in tether net/gripper systems. Multibody Syst Dyn, 2004, 11: 235–250
13 Meng Z, Wang D, Yang Y, et al. Release dynamic and control for tethered space robot using CMAC. In: Proceedings of the 6th IEEE Conference on Industrial Electronics and Applications. IEEE, 2011
14 Wang D, Huang P, Meng Z, et al. Coordinated attitude control of the combination system after target capture by a tethered space robot (in Chinese). Acta Aeronaut Astronaut Sin, 2013, 34: 1998–2006
15 Zhai G, Qiu Y, Liang B, et al. On-orbit capture with flexible tether-net system. Acta Astronaut, 2009, 65: 613–623
16 Chen Q, Yang L P. On dynamics of casting a net structure of flexible cables on orbit. In: Proceedings of the 60th International Astronautical Congress. Daejeon: AIAA, 2009
17 Yu Y, Baoyin H X, Li J F. Dynamic modelling and analysis of space webs. Sci China Phys Mech Astron, 2011, 54: 783–791
18 Bonnal C, Ruault J M, Desjean M C. Active debris removal: recent progress and current trends. Acta Astronaut, 2013, 85: 51–60
19 Bremen A S. Robotic geostationary orbit restorer (ROGER) phase A final report. ESA Contract No.: 15706/01/NL/WK, 2003
20 Krupa M, Poth W, Schagerl M, et al. Modelling, dynamics and control of tethered satellite systems. Nonlinear Dynam, 2006, 43: 73–96
21 Ellis J R. Modeling, Dynamics, and Control of Tethered Satellite Systems. Blacksburg, Virginia: Virginia Polytechnic Institute and State University, 2010
22 Wang S, Shang H B, Wu W R. Interplanetary transfers employing invariant manifolds and gravity assist between periodic orbits. Sci China Tech Sci, 2013, 56: 786–794
23 Cho S, Mcclamroch N H. Optimal orbit transfer of a spacecraft with fixed length tether. J Astronaut Sci, 2003, 51: 195–204
24 Sun L, Zhao G W, Huang H, et al. Analysis of librational and vibrational characteristics for tethered system during orbital transfer in plane (in Chinese). Acta Aeronaut Astronaut Sin, 2011, 33: 1245–1254
25 Zhao G, Sun L, Tan S, et al. Librational characteristics of a dumbbell modeled tethered satellite under small, continuous, constant thrust. P I Mech Eng G - J Aer, 2012, 227: 857–872
26 Sun L, Zhao G, Huang H. Stability and control of tethered satellite with chemical propulsion in orbital plane. Nonlinear Dynam, 2013, 74: 1113–1131
27 Liu H T, Yang L P, Zhang Q B, et al. An investigation on tether-tugging de-orbit of defunct geostationary satellites. Sci China Tech Sci, 2012, 55: 2019–2027
28 Jasper L, Schaub H, Seubert C, et al. Tethered tug for large low earth orbit debris removal. In: Proceedings of the AAS/AIAA Astrodynamics Specialists Conference. Charleston: AIAA, 2012
29 Jasper L, Schaub H. Input Shaped large thrust maneuver with a tethered debris object. Acta Astronaut, 2014, 96: 128–137
30 Aslanov V, Yudintsev V. Dynamics of large space debris removal using tethered space tug. Acta Astronaut, 2013, 91: 149–156
31 Aslanov V S, Yudintsev V V. Dynamics of large debris connected to space tug by a tether. J Guid Control Dynam, 2013, 36: 1654–1660
32 Aslanov V S, Ledkov A S. Dynamics of towed large space debris taking into account atmospheric disturbance. Acta Mechanica, 2014: 1–13
33 Tang Q G, Zhang Q B, Yang T, et al. Dynamics of Terminal Correction Submunition (in Chinese). Beijing: National Defense Industry Press, 2013
34 Zhang S H, Zhao H, Du A M, et al. 3-D numerical calculation of magnetic drag parachute. Sci China Tech Sci, 2013, 56: 2059–2065
35 Lin K P, Luo Y Z, Zhang J, et al. Planning for space station long-duration orbital mission under multi-constraints. Sci China Tech Sci, 2013, 56: 1075–1085
36 Cai W W, Yang L P, Zhu Y W, et al. Formation keeping control through inter-satellite electromagnetic force. Sci China Tech Sci, 2013, 56: 1102–1111
37 Zhu R Z, Wang X G. Continuous constant thrust maneuver in polar coordinate systen. Spacecraft Eng, 2008, 17: 31–37
38 Inter-Agency Space Debris Cordination Committee. IADC Space Debris Mitigation Guidelines, IADC-02-01 Revision 1, 2007
39 Cosmo M L, Lorenzini E C. Tethers in Space Handbook. Cambridge, Massachusetts: Smithsonian Astrophysical Observatory, 1997